JOURNAL OF APPLIED CRYSTALLOGRAPHY
ISSN 1600-5767

Crystal growth of Ru-doped congruent $LiNbO_3$ and investigation of crystalline perfection and optical properties

B. Riscob,[a]* Indranil Bhaumik,[b] S. Ganesamoorthy,[c] R. Bhatt,[b] N. Vijayan,[d] Khavangkhui Zimik,[e] A. K. Karnal,[b] G. Bhagavannarayana[d,f]* and P. K. Gupta[b]

[a]Institute for Plasma Research, Bhat, Gandhinagar, Gujarat 382 428, India, [b]Laser Materials Development and Device Division, RRCAT, Indore, Madhya Pradesh 452 013, India, [c]Materials Science Group, IGCAR, Kalpakkam, Tamil Nadu 603 102, India, [d]CSIR-National Physical Laboratory, Crystal Growth and X-ray Analysis, New Delhi 110 012, India, [e]Laser Science and Technology Centre, Defence Research and Development Organization, Delhi 110 054, India, and [f]Department of Physics, K L University, Green Fields, Vaddeswaram, Guntur District, Andhra Pradesh 522 502, India. *Correspondence e-mail: riscob@gmail.com, bhagavanna55@gmail.com, bhagavan@nplindia.org

Received 3 February 2015
Accepted 2 October 2015

Edited by G. Renaud, CEA-Grenoble DSM/INAC/SP2M/NRS, Grenoble, France

Keywords: crystal growth; high-resolution X-ray diffractometry; rocking curves; lithium niobate.

Single crystals of undoped and Ru-doped congruent $LiNbO_3$ (LN) were successfully grown by the Czochralski method. The axial and radial gradient of the radio frequency furnace was controlled in order to obtain crack-free single crystals. Wafers were cut from the grown Ru-doped single crystal at different axial positions along the growth direction and subjected to various characterization analyses. Good optical homogeneity and low residual strain in the grown crystal is confirmed by the conoscopy patterns. Further, it is confirmed that Ru doping does not influence the optical sign of the crystal. From a high-resolution X-ray diffractometry analysis, it is evident that the as-grown undoped LN crystal exhibited better crystalline perfection with a single and sharp diffraction curve in comparison to the Ru-doped crystals, which are characterized by a broader diffraction curve. Absorption coefficient and band-gap analysis across the axial length revealed a concentration variation of Ru across the length. Refractive index measurements carried out using a prism coupler showed variation in the optical birefringence, also due to the variation of Ru concentration at different positions of the grown single crystal.

1. Introduction

Today's technology requires high-quality defect-free bulk size single crystals for device fabrication in various applications (Riscob *et al.*, 2012). Nonlinear optical materials have been playing an increasingly important role in the field of laser science and technology (Cyranoski, 2009; Chen *et al.*, 2005; Riscob *et al.*, 2014). Lithium niobate ($LiNbO_3$; LN) single crystals are one of the potential nonlinear optical materials and have been extensively used for electro-optic, acousto-optic and piezoelectric applications. Good quality bulk LN crystals are grown from the congruent melt composition (Li/Nb $\simeq$ 0.94) using the Czochralski method (Byer, 1970; Riscob, Bhaumik *et al.*, 2013). They are also important for high-energy lasers required for inertial confinement fusion research (Zaitseva & Carman, 2001), colour displays, electro-optic switches, holographic data storage, frequency conversion *etc.* (Badan *et al.*, 1993). Pristine LN crystals exhibit a photorefractive effect in both the stoichiometric and non-stoichiometric form. But, the efficiency of the effect can be improved significantly on adding selected dopants into the crystalline matrix during the growth. Different transition metal ions, such as Fe (Hesselink *et al.*, 1998), Mn (Yang *et al.*, 2003), Cu (Imbrock *et al.*, 2002) and Ce (Yang *et al.*, 2000), have been

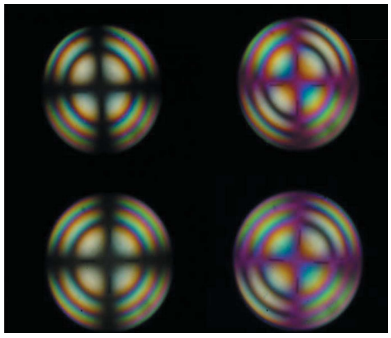

© 2015 International Union of Crystallography

tried as dopants by various researchers to enhance the photorefractive property. Among these, Fe is found to be a better choice for improving the photorefractive effect of LN. However, iron in a grown crystal can attain two valance states, namely Fe^{2+} or Fe^{3+} (Kong *et al.*, 2008). As a result, the photorefractive effect and other properties of LN vary according to the valance state of the dopants present in the crystal. Researchers have put their efforts into searching for new dopants for improving the photorefractive effect of LN. Ruthenium (Ru) is a good choice in this context, as revealed for many host materials such as $Bi_{12}TiO_{20}$, strontium barium niobate, $Bi_4Ge_3O_{12}$ and $Bi_{12}SiO_{20}$ (Marinova *et al.*, 2002, 2003; Fujimura *et al.*, 2002; Ramaz *et al.*, 2005). However, the main challenge of growing Ru-doped LN crystals is to maintain the concentration homogeneity along the growth length. The evaporation temperature of Ru is much lower (~1073 K) than the melting point of LN (~1526 K), and as a result, during the growth, the dopant concentration decreases from the seed portion to the bottom portion of the crystal. Further, during the post-growth cooling cycle, LN single crystals undergo a para- to ferroelectric phase transition at ~1413 K, associated with a volume change, and hence it is very common that these crystals contain internal structural grain boundaries (Bhagavannarayana, Ananthamurthy *et al.*, 2005). Crystalline quality has become a very stringent requirement owing to miniaturization of devices, and hence evaluation of crystalline perfection by an appropriate method is of immense importance in LN crystals. In one of our recent studies on LN crystals, it was found that post-growth thermal annealing with slow heating and cooling rates (2–5 K h^{-1}) improves the crystalline perfection significantly, leading to an enhancement in the optical and piezoelectric properties (Bhagavannarayana, Budakoti *et al.*, 2005).

In the present investigation, undoped and Ru-doped LN crystals were grown successfully under an optimized post-growth cooling cycle to minimize the structural defects. The well proven nondestructive high-resolution X-ray diffraction (HRXRD) technique using an in-house-developed high-resolution multi-crystal X-ray diffractometer is used to evaluate the crystalline perfection of the grown undoped and Ru-doped LN crystals. The spectroscopic properties, optical band gap and refractive index of Ru-doped LN at two different positions are also evaluated. To assess the variation of Ru concentration from top to bottom of the grown crystal boule, two samples prepared from the top and bottom portions of the boule were characterized by energy-dispersive X-ray spectroscopy (EDXS).

2. Experimental details

2.1. Crystal growth

Li_2CO_3 (99.999%) and Nb_2O_5 (99.99%) were used as the raw materials and weighed in the molar ratio of 48.46:51.54 to obtain the congruent composition. For Ru-doped crystals, 0.02 wt% RuO_2 (99.99%) was added to the charge. Before weighing, all the chemicals were dried to get rid of the moisture absorbed in them. The raw materials, except RuO_2, were mixed thoroughly by the ball-milling process using zirconia balls in a Turbo mixer. The mixed materials were transferred into a platinum crucible and heated at 1173 K for 20 h for solid state reaction to form LN. Then, the calcined materials were ground and milled again, with the addition of RuO_2 in the case of the doped crystal, and used for the crystal growth experiment. Addition of RuO_2 at the final stage helps in reducing the evaporation of Ru in the starting chemical.

A Cyberstar automatic diameter controlling Czochralski crystal puller coupled with a Huttinger induction heating system (8 kHz, 50 kW) was used for the crystal growth experiments. The growth temperatures were controlled by using a Eurotherm 902 (single loop) PID-based programmable temperature controller with a resolution of ±0.01 K *via* an R-type thermocouple. Normally, induction heating systems have high radial and axial temperature gradients that lead to the formation of cracks in the crystal during growth, as well as while the grown crystal is being detached from the melt. To obtain crack-free crystals with a flat interface, the ratio of axial and radial temperature gradient should be kept high. So, it is advisable to use additional thermal shields to obtain a good quality crystal. In the present furnace setup, we used layers of different thermal insulators such as alumina and zirconia tubes to minimize the temperature loss. A schematic representation of the same is shown in Fig. 1. In addition to the thermal insulation assembly, an after-heater made of platinum foil of nearly 100 mm height was placed above the crucible. The prepared charge was transferred to a platinum crucible of 50 mm diameter and 50 mm height. The material was melted completely and the charge was homogenized at a temperature elevated by 50 K above the melting temperature for only

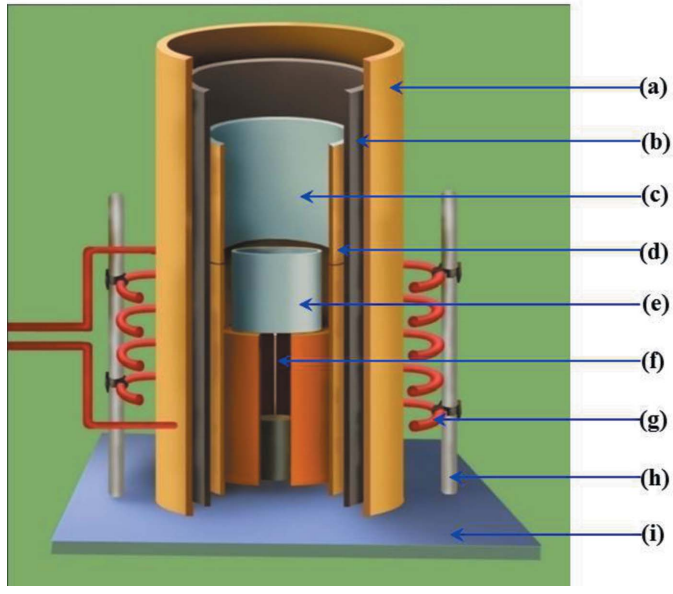

Figure 1
Model of the furnace used for crystal growth. (a) Outer zirconia tube, (b) inner refractory, (c) platinum foil, (d) inner zirconia tube, (e) platinum crucible, (f) thermocouple, (g) radio frequency heating coil, (h) heating coil support and (i) high-temperature glass wool base.

15 min as Ru has a tendency to evaporate from the charge. A [001]-oriented seed was used for the growth, and the seeding was done using the technique described elsewhere Riscob, Bhaumik *et al.*, 2013; Bhaumik *et al.*, 2002). Subsequently, growth of the crystal was achieved using an automatic diameter controlling mode. During the growth of the constant diameter part of the crystal, the pulling and rotation rates were kept at 5 mm h^{-1} and 25 r min^{-1}, respectively. After the completion of the growth, the grown crystal was slowly cooled across the phase transition temperature (1423 K) at a rate of 20 K h^{-1} down to 1323 K and then cooled at a rate that was increased step by step down to room temperature.

The grown doped crystal is yellow–red in colour because of the inclusion of Ru (Fig. 2), and the dimensions of the crystal are 25 mm diameter and 30 mm length. By using EDXS the concentration of the Ru was confirmed: it varies from 0.015 to 0.003 wt% from the top to bottom of the crystal.

2.2. Conoscopy study

To characterize the homogeneity of the grown Ru-doped crystal, a conoscopy study was carried out using an OLYMPUS BX-60 polarized light optical microscope under crossed polarization conditions. Optically polished [001]-oriented (along optic axis) samples were used for the measurement.

2.3. High-resolution X-ray diffraction

The crystalline perfection of the grown single crystals was characterized by HRXRD by employing a multi-crystal X-ray diffractometer developed at the National Physical Laboratory (Lal & Bhagavannarayana, 1989). The well collimated and monochromated bMo $K\alpha_1$ beam obtained from three monochromator Si crystals set in a dispersive (+,−,−) configuration was used as the exploring X-ray beam. The specimen crystal was aligned in the (+,−,+) configuration. Owing to the dispersive configuration, though the lattice constant of the monochromator crystal(s) and the specimen are different, the unwanted dispersion broadening in the diffraction curve (DC) of the specimen crystal is insignificant. The specimen was rotated around the vertical axis, which is perpendicular to the plane of diffraction, with an angular interval of 0.4″. The rocking or diffraction curves were recorded by changing the glancing angle (angle between the incident X-ray beam and the surface of the specimen) around the Bragg diffraction peak position θ_B (taken as zero for the sake of convenience), starting from a suitable arbitrary glancing angle and ending at a glancing angle after the peak so that all the meaningful scattered intensities on both sides of the peak could be included in the diffraction curve. The DC was recorded by the so-called ω scan method, wherein the detector is kept at the same angular position $2\theta_B$ with a wide opening for its slit. This arrangement is very appropriate to record the short range order scattering caused by defects or by the scattering from local Bragg diffraction from agglomerated point defects or due to low angle and very low angle structural grain boundaries (Bhagavannarayana & Kushwaha, 2010; Senthi Kkumar *et al.*, 2011). Before recording the diffraction curve, to remove the surface damage that occurred during cutting of the sample and to polish the surface, the samples were ground, lapped and then etched with a non-preferential etchant of HNO_3 and HF in a 2:1 ratio at room temperature for 10 min.

Figure 2
The Ru-doped $LiNbO_3$ single crystal grown along [001].

2.4. Raman spectroscopy

A [001] single-crystal plate was examined with a HORIBA-T64000 Triple Raman spectrometer to carry out the investigation of the molecular vibrations in the wavenumber range 100–1000 cm^{-1} at 293 K. A 514.5 nm Ar^+ laser (Spectra Physics) with a beam power of 80 mW was used as excitation source.

2.5. UV–vis–NIR spectroscopy

The optical transmission and absorption spectra were recorded in the UV–vis–NIR region of the specimen using a commercial spectrophotometer (Jasco V-263). The measurements were carried out with unpolarized light at normal incidence at room temperature. For the measurement, cut and polished samples of thickness 1 mm were used.

2.6. Refractive index measurement

A prism coupling based refractive index measurement system (Metricon Corporation, model 2010/M) was used. The index calibration of the instrument was done with standard fused silica (ICS 14) and subsequently the experimental error was estimated by comparing the measured refractive index of Schott LASF18A with the data sheet. The error was found to be within 1×10^{-3}. Details of the experiment are described by Bhaumik *et al.* (2011).

3. Results and discussion

3.1. Conoscopy patterns

The conoscopy patterns of the plates obtained from the top and the bottom portions of the doped crystal, observed under a polarized light optical microscope, are shown in Figs. 3(*a*) and 3(*b*), respectively. The patterns are characterized by concentric circular rings, signifying the homogeneity of the grown crystals along the radial directions. Further, in order to determine the optical sign of the crystal, an accessory wave-plate (λ plate, 530 nm) was introduced into the optical path. The appearance of the blue colour in the second and fourth quadrants indicates that the crystal is of negative uniaxial (Figs. 3*c* and 3*d*) type.

3.2. High-resolution X-ray diffractometry

Fig. 4 shows the high-resolution DCs recorded for a set of three LN crystals using the (006) diffracting planes in symmetrical Bragg geometry with bMo $K\alpha_1$ radiation. The curves (*a*), (*b*) and (*c*) are, respectively, for (*a*) an undoped crystal cut from the middle portion of the as-grown boule, (*b*) an Ru-doped LN crystal cut from the top portion (close to the seed crystal) of the boule and (*c*) an Ru-doped LN crystal cut from the bottom portion of the boule. As seen in the figure, the DCs of all the specimens contain a single diffraction peak without any satellite peak, showing that these crystals do not contain any internal structural grain boundaries which are otherwise very common in LN crystals (Bhagavannarayana, Ananthamurthy *et al.*, 2005). Though all the DCs have single curves, there are some interesting and distinctive features in these curves. The full width at half-maximum (FWHM) of curve (*a*) is ∼29″. Though this value is somewhat more than that expected from the plane wave theory of dynamical X-ray diffraction (Batterman & Cole, 1964), *i.e.* 2.6″ (Kushwaha *et al.*, 2011), it is comparable to the earlier reported values of 21″ (Bhatt *et al.*, 2011) and 62″ (Kushwaha *et al.*, 2012). This indicates the presence of a low density of point defects and

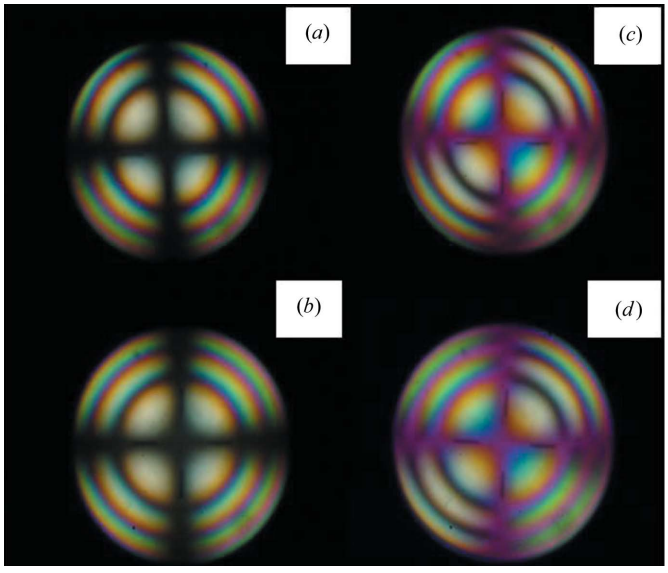

Figure 3
(*a*), (*b*) The conoscopy patterns for Ru:LN crystals from the top and bottom portions, respectively. (*c*), (*d*) Insertion of a retarding λ waveplate changed the colour of the second and fourth quadrants from yellow to blue (lower wavelength side), revealing that the crystal is of negative uniaxial type.

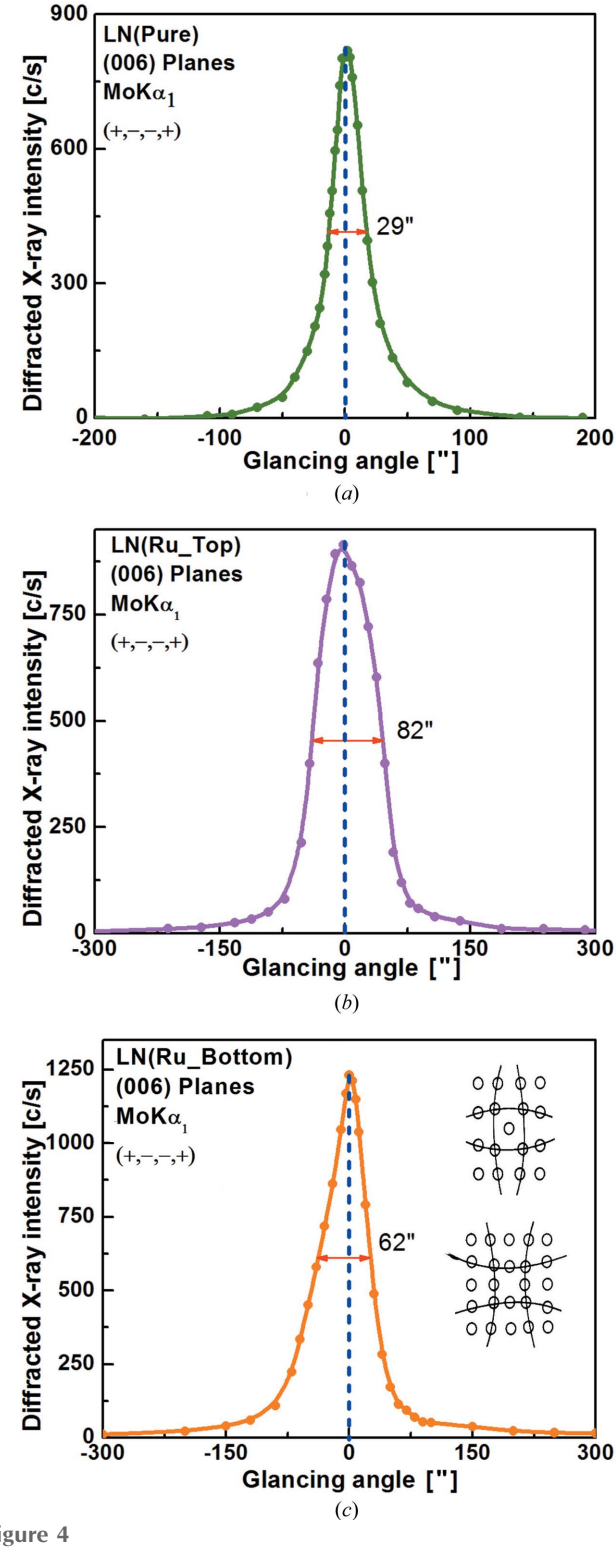

Figure 4
Diffraction curves recorded for LN single crystals using (006) diffracting planes with bMo $K\alpha_1$ radiation: (*a*) undoped specimen cut from the middle portion of the boule, (*b*) Ru-doped specimen cut near the seed and (*c*) Ru-doped specimen cut near the bottom.

their aggregates, which are unavoidable in real crystals owing to thermodynamical effects. The FWHM of curve (*b*) is ∼82″, and this value is substantially higher than that of the undoped crystal, indicating that Ru doping leads to a substantial increase of point defects. The FWHM value of ∼62″ of curve (*c*) belonging to the specimen close to the bottom of the ingot is, however, slightly less than that of the specimen taken from the top portion, which may be due to a lower concentration of Ru dopants at the bottom portion of the crystal as observed by EDXS. However, this value is also quite high in comparison to that of the undoped crystal, showing that the overall density of point defects arising from the doping is less than that of curve (*b*). There are some interesting features in the shape of the DC. The DC is quite asymmetric with respect to the Bragg peak position. For a particular angular deviation ($\Delta\theta$) of glancing angle (θ) with respect to the Bragg peak position (taken as zero for the sake of convenience), the scattered intensity is much more in the negative direction in comparison to that of the positive direction. This feature clearly indicates that the crystal contains predominantly vacancy-type defects over interstitial defects. This can be well understood by the fact that owing to vacancy defects the lattice around these defects undergoes tensile stress (Bhagavannarayana *et al.*, 2008) and the lattice parameter *d* (interplanar spacing) increases. This leads to more scattered (also known as diffuse X-ray scattering) intensity at slightly lower Bragg angles (θ_B) as *d* and $\sin\theta_B$ are inversely proportional to each other in the Bragg equation ($2d\sin\theta_B = n\lambda$; *n* and λ being the order of reflection and wavelength, respectively, which are fixed). The inset in the curve shows a schematic to illustrate how the lattice around the defect core undergoes tensile stress. The converse explanation is true in the case of interstitial defects, which cause compressive stress in the lattice around the defect core, leading to a decrease of lattice spacing and in turn resulting in more scattered intensity at the higher Bragg angles. It may be mentioned here that the variation in the lattice parameters is confined very close to the defect core, which gives only the scattered intensity close to the Bragg peak. Long range order would not be expected and hence a change in the lattice parameter is also not expected (Bhagavannarayana & Kushwaha, 2010). It may be worth mentioning here that the defects are more or less uniformly distributed in the crystal. If the defects were distributed randomly as macroscopic clusters, then the strain generated by such clusters would have been large, leading to cracks and structural grain boundaries, which can be seen very clearly in HRXRD curves with additional peak(s) as observed in one of our recent studies on urea-doped crystals in tristhioureazinc(II) sulfate (Bhagavannarayana & Kushwaha, 2010). However, in the present experiments the diffraction curve does not contain any additional peak that indicates the absence of clustering of point defects at a macroscopic level. The single diffraction peak with reasonably low FWHM values of even Ru-doped crystals indicates that the crystalline perfection in the doped crystal is quite good. The above results for the top and bottom specimens indicate that Ru ions are accommodated in the crystal lattice with less strain in the crystal. The difference in the shape and FWHM values of the plates from different axial positions reveals that the Ru concentration at interstitial positions is lower in the case of the specimen taken from the bottom portion, which is confirmed from the EDXS studies. This could be because of the gradual decrease of Li as well as Ru concentration during the growth process due to evaporation of Ru. The decrease of Li concentration has been observed in our earlier studies (Bhagavannarayana, Budakoti *et al.*, 2005; Bhagavannarayana, Kushwaha *et al.*, 2011). The decrease in Li^+ concentration led to antisitic defects (Ru_{Li}^{1+}) formed by the replacement of two Li^{1+} ions by one Ru^{2+} ion in $LiNbO_3$ single crystals for charge neutrality, leading to the formation of one extra vacancy in addition to the already existing vacancies, which may be the reason for the predominance of vacancy defects in the bottom specimen [curve (*c*)].

3.3. Raman analysis

Raman spectroscopy is used as an efficient tool for characterizing the intrinsic and extrinsic defects of LN single crystals (Mignoni *et al.*, 2010; Sidorov *et al.*, 2007). The Raman measurements of Ru:LN samples obtained from the top and the bottom of the grown crystal were carried out in the *Z*(*YX*)*Z* scattering configuration and the results are shown in Fig. 5. The spectra are characterized by several peaks corresponding to different vibration modes. The observed peaks at 152 and 872 cm^{-1} are due to the E(TO1) and E(LO9) modes of Nb—O vibrations. The Li—O and oxygen octahedron (O—O) vibrations observed at 365 and 580 cm^{-1} are due to the E(TO6) and E(TO8) modes (Caciuc *et al.*, 2000). There is also a weak Raman band at around 682 cm^{-1}, which is attributed to the vibrations of E(TO9) and E(LO8) normal modes (Hermet *et al.*, 2007). A variation in the peak intensities is observed for the top and bottom wafers, but no shift in the peak position is observed, signifying that there is no structural change except for the change in the concentration of point defects, which are observed by HRXRD measurements. The observed variation

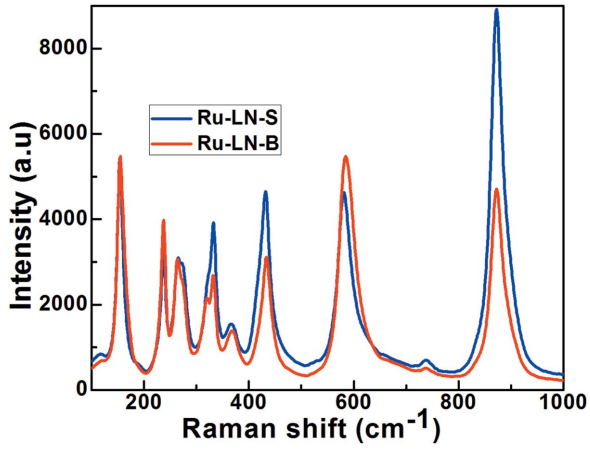

Figure 5
Raman spectra of Ru:LN samples obtained from the top and the bottom of the grown crystal were obtained in the *Z*(*YX*)*Z* scattering configuration.

in the intensities of the Raman peaks in both specimens suggests that there is a variation in the dopant concentration, which is consistent with the band gap and refractive index results described in the forthcoming sections. Further, the LO modes at 872 cm^{-1} are used to analyse the concentration of lithium (C_{Li}) present in the crystal by using an empirical formula: C_{Li} [mol%] = 53.29 − 0.1837Γ [cm^{-1}], where Γ stands for the line width (FWHM) of the peak at particular positions (Schlarb *et al.*, 1993). As calculated using the Raman peaks at 872 cm^{-1}, the wafer from the top portion of the crystal has 47.942 mol% Li_2O content, which suggests that Ru might have replaced Li in the lattice. But, the wafer from the bottom portion has 48.117 mol% Li_2O, suggesting that there might be a reduction in the Ru concentration due to evaporation of Ru during the growth experiment.

3.4. UV–vis–NIR transmission analysis

Fig. 6(*a*) shows the transmittance spectra of the top and the bottom portions of the Ru-doped LN single crystal. The transmittance spectra were recorded in the wavelength range of 200–1200 nm. Fig. 6(*b*) shows the absorption coefficient of the Ru:LN samples. The recorded spectra showed that both the samples exhibited optical transparency above 350 nm. However, there is broad absorption above 350 nm centred at ∼370 and ∼530 nm, which is due to the transitions of unshielded valance electrons of Ru ions in the crystal field of LN. It is noteworthy that the dopant Ru ions have three possible different valance states, Ru^{3+}, Ru^{4+} and Ru^{5+}, but the correlation between the absorption peak position and the valance state of Ru is not yet established (Ramaz *et al.*, 2005). From the plot it is evident that the magnitude of the absorption band is different for both the samples, with the samples prepared close to the top showing stronger absorption. This variation is due to the concentration variation of Ru content in the crystal along the growth direction because of the evaporation of Ru.

A similar absorption peak is observed around 480 nm in the case of Fe-doped LN samples due to the Fe^{2+} ions (Lee *et al.*, 2001). Further, a shift in the UV cutoff is observed in the present case. This may be attributed to impurity-induced band tailing as well as broad absorption of Ru ions spanning from

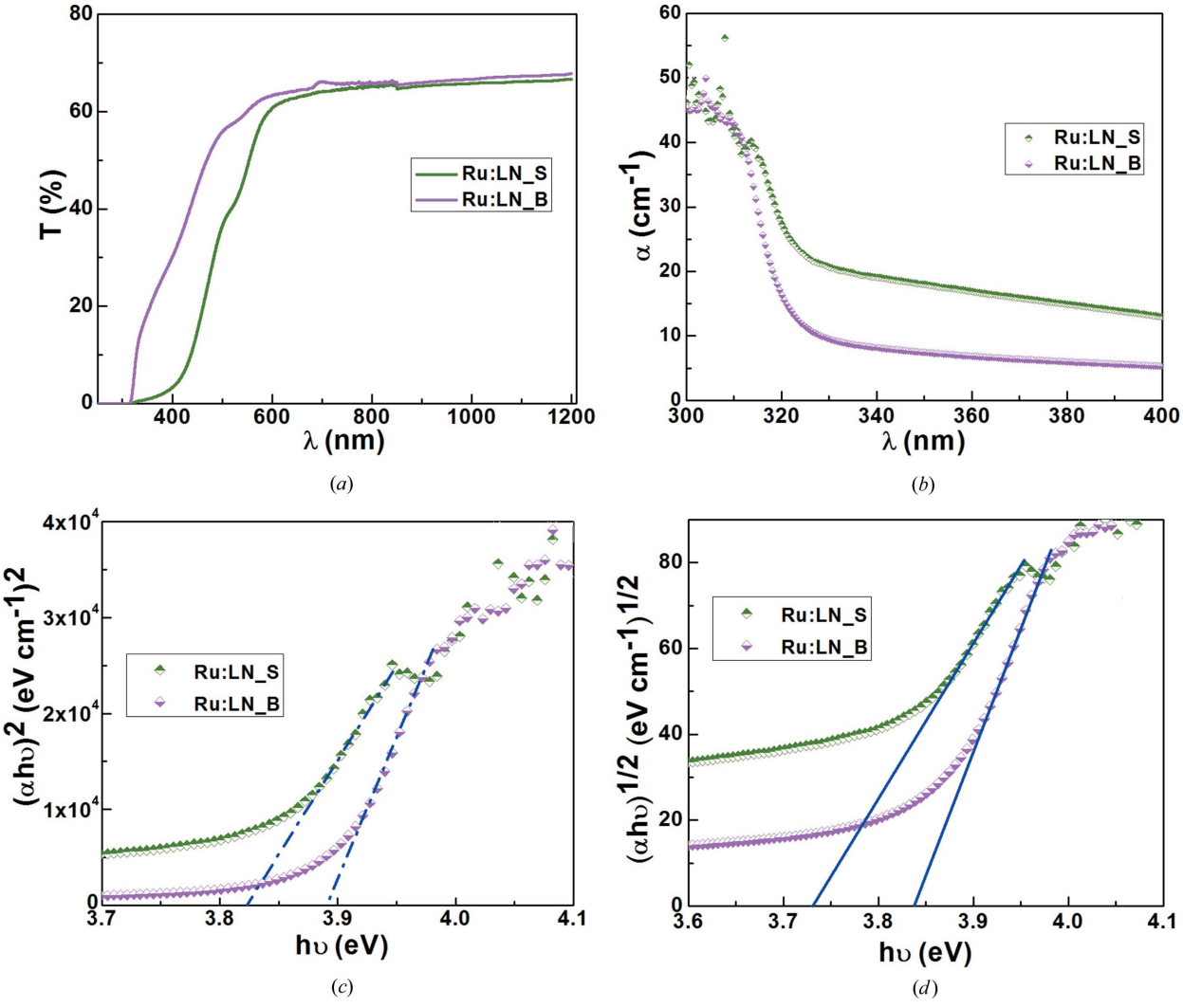

Figure 6
(*a*) UV–vis–NIR transmission spectra, (*b*) absorption coefficient, (*c*) plot of direct band gap and (*d*) plot of indirect band gap of Ru:LN single crystals.

the visible to the band edge. A shift in the band edge is reported by various authors in the case of Fe-doped LN with a variation of dopant concentration (Bhatt *et al.*, 2013; Pracka *et al.*, 1999).

The direct and indirect band-gap energies are estimated using the empirical relation $\alpha h\nu \propto (h\nu - E_g)^m$ (Taue, 1972), where $h\nu$ is the photon energy, E_g is the band-gap energy and m is an exponent determined by the nature of electron transition during the absorption process, *i.e.* $m = 1/2$ for direct transition and $m = 2$ for indirect transition. Fig. 6(*c*) shows a plot of $(\alpha h\nu)^2$ *versus* $h\nu$ which provides a detailed view of the direct band-gap (E_g^d) transition. The steep rise of absorption and its linear fit at higher photon energy depicts the direct allowed interband transition. The intercept of the fitted straight line with the energy axis gives its direct band-gap energy. The estimated band gaps of the samples cut from the top and the bottom portions of the Ru:LN samples are ~3.82 and 3.89 eV, respectively, which are less than the value (4.12 eV) reported for undoped congruent LN (Bhatt *et al.*, 2012). Fig. 6(*d*) shows the plot of $(\alpha h\nu)^{1/2}$ *versus* $h\nu$, where the intercept of the fitted straight line with the energy axis gives the indirect band-gap energy (E_g^{ind}). The estimated indirect band gaps of the samples cut from the top and the bottom portions of the Ru:LN samples are ~3.73 and 3.84 eV, respectively. The indirect band-gap energy estimated for undoped LN is ~3.95 eV (Bhatt *et al.*, 2012). The redshifts in both the direct and the indirect band transitions in the Ru-doped sample are a typical characteristic of transition metal impurity due to their broad impurity–impurity level transitions and intrinsic defects. A similar observation is also reported in Fe-doped samples (Kushwaha *et al.*, 2011).

3.5. Refractive index

The ordinary (n_o) and extraordinary (n_e) refractive indices (RIs) of the Ru:LN samples and the undoped LN crystal of the same composition (Li/Nb) were measured by the prism coupling technique. Measurements were carried out at two different wavelengths, 532 and 1064 nm. The measured ordinary and extraordinary refractive indices of Ru:LN at 1064 nm for the top and bottom samples are found to be slightly less than that of the undoped LN sample. But, at 532 nm both the ordinary and the extraordinary refractive indices are found to be higher than that of undoped LN. A small deviation in the refractive indices is observed in the top and bottom portions of the crystals. The fact that the top portion of the crystal has slightly higher indices indicates a higher concentration of Ru. The value of the RI is slightly higher at 532 nm and slightly lower at 1064 nm for the sample prepared from the top part of the crystal. This may be attributed to the absorption band at 490 nm due to Ru, which influences the RI measured at 532 nm. Similar results are observed in Fe-doped LN (Kushwaha *et al.*, 2011) and Zr-Fe:LN (Riscob, Bhatt *et al.*, 2013). This shows that the Ru dopant is a promising material for photorefractive application. The birefringence ($\Delta n = n_e - n_o$) value of undoped LN was found to be higher at 532 nm than that of 1064 nm and the same trend is observed in the case of Ru-doped samples as well (Figs. 7*a* and 7*b*). The birefringence plot as shown in Fig. 7(*c*) shows that the birefringence decreased to a great extent for the sample from the top as compared to the bottom sample at 532 nm, owing to the increase of absorption in the top sample. In the case of 1064 nm, the difference in the

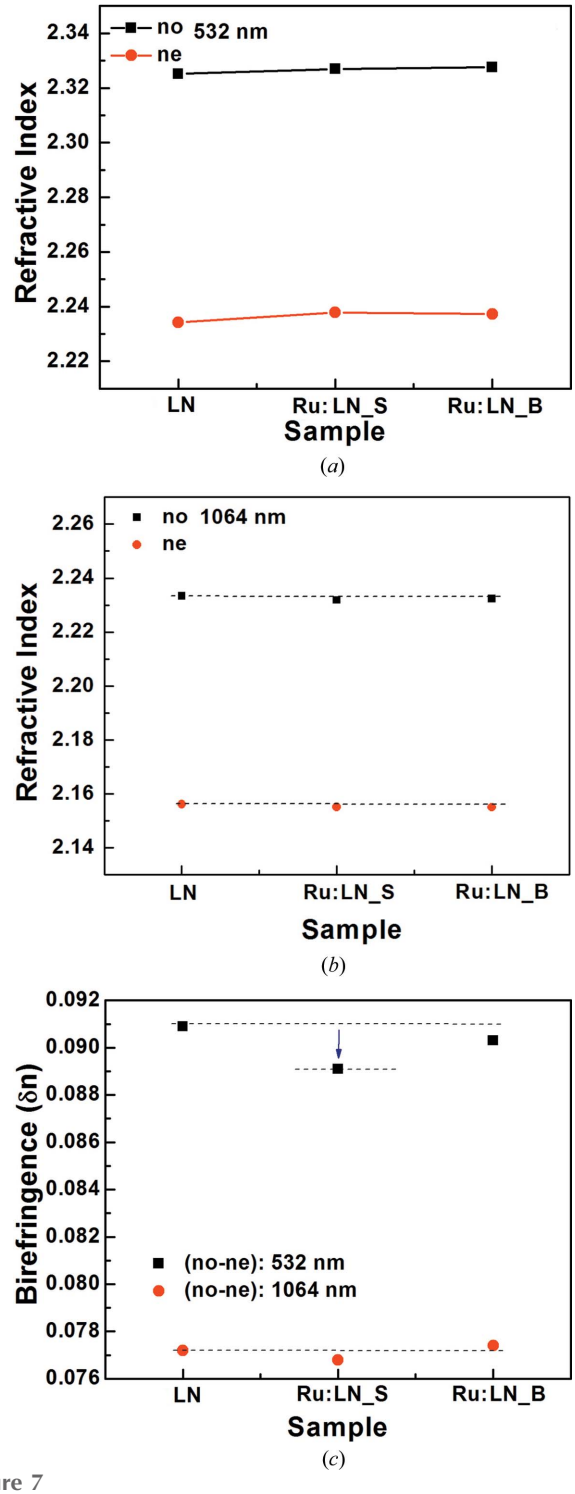

Figure 7
Refractive index of Ru:LN single crystals from the top and bottom portions at two different wavelengths: (*a*) 532 nm, (*b*) 1064 nm. (*c*) Birefringence of Ru:LN.

birefringence value between the undoped and Ru-doped specimens is not significant, but it followed a trend similar to that for 532 nm. The value of birefringence of the sample from the bottom portion is closer to the undoped LN results. This observation clearly signifies that the RI of LN is influenced by Ru doping in the visible region where the impurity–impurity or impurity–band transition is dominant.

4. Conclusion

A good quality Ru-doped LN single crystal was grown under optimized conditions using an inductive heating furnace. The conoscopy patterns at different positions of the grown crystal confirm its optical homogeneity. The HRXRD curve of the grown crystal at different postions confirmed that the crystal is free from grain boundaries but contains point defects. The variation of FWHM in the XRD peak observed for crystal plates cut from the top and bottom portions of the grown crystal is due to the concentration variation of Ru in the crystal. Raman studies clearly depict the variation of Li content in the sample but show no signature of any structural change. A band-gap analysis reveals that incorporation of Ru led to a decrease in the band gap. The observed absorption band due to Ru for two different samples of the same crystal suggests a concentration variation of Ru in the grown crystal. The high birefringence value at lower wavelength and the low value at higher wavelength of the sample cut from the top portion suggest that a good amount of Ru doping concentration improves the holographic data storage ability of the material as compared to an undoped sample.

Acknowledgements

The authors acknowledge B. K. Sajith and A. Saxena, RRCAT, for their technical support during crystal growth activity. The authors acknowledge Dr A. K. Bandyopadhyay, NPL, New Delhi, for extending the Raman measurement facility.

References

Badan, J., Hierle, R., Perigaud, A., Zyss, J. & Williams, D. J. (1993). Editors. *NLO Properties of Organic Molecules and Polymeric Materials*, American Chemical Symposium Series Vol. 233. Washington, DC: American Chemical Society.
Batterman, B. W. & Cole, H. (1964). *Rev. Mod. Phys.* **36**, 681–717.
Bhagavannarayana, G., Ananthamurthy, R. V., Budakoti, G. C., Kumar, B. & Bartwal, K. S. (2005). *J. Appl. Cryst.* **38**, 768–771.
Bhagavannarayana, G., Budakoti, G. C., Maurya, K. K. & Kumar, B. (2005). *J. Cryst. Growth*, **282**, 394–401.
Bhagavannarayana, G. & Kushwaha, S. K. (2010). *J. Appl. Cryst.* **43**, 154–162.
Bhagavannarayana, G., Kushwaha, S. K., Shakir, Mohd & Maurya, K. K. (2011). *J. Appl. Cryst.* **44**, 122–128.
Bhagavannarayana, G., Parthiban, S. & Meenakshisundaram, S. (2008). *Cryst. Growth Des.* **8**, 446–451.
Bhatt, R., Bhaumik, I., Ganesamoorthy, S., Karnal, A. K., Swami, M. K., Patel, H. S. & Gupta, P. K. (2012). *Phys. Status Solidi A*, **209**, 176–180.
Bhatt, R., Ganesamoorthy, S., Bhaumik, I., Karnal, A. K., Bhagavannarayana, G. & Gupta, P. K. (2011). *J. Optoelectron. Adv. Mater.* **13**, 245–250.
Bhatt, R., Ganesamoorthy, S., Bhaumik, I., Sexana, A., Karnal, A. K., Gupta, P. K., George, J. & Ranganathan, K. (2013). *Opt. Laser Technol.* **50**, 112–117.
Bhaumik, I., Bhatt, R., Ganesamoorthy, S., Saxena, A., Karnal, A. K., Gupta, P. K., Sinha, A. K. & Deb, S. K. (2011). *Appl. Opt.* **50**, 6006–6010.
Bhaumik, I., Ganesamoorthy, S., Bhatt, R., Sundar, R., Karnal, A. K. & Wadhawan, V. K. (2002). *J. Cryst. Growth*, **243**, 522–525.
Byer, R. L. (1970). *J. Appl. Phys.* **41**, 2320–2325.
Caciuc, V., Postnikov, A. V. & Borstel, G. (2000). *Phys. Rev. B*, **61**, 8806–8813.
Chen, C., Lin, Z. & Wang, Z. (2005). *Appl. Phys. B*, **80**, 1–25.
Cyranoski, D. (2009). *Nature*, **457**, 953–955.
Fujimura, R., Kubota, E., Matoba, O., Shimura, T. & Kuroda, K. (2002). *Opt. Commun.* **213**, 373–378.
Hermet, P., Veithen, M. & Ghosez, P. (2007). *J. Phys. Condens. Matter*, **19**, 456202.
Hesselink, L., Orlov, S. S., Liu, A., Akella, A., Lande, D. & Neurgaonkar, R. R. (1998). *Science*, **282**, 1089–1094.
Imbrock, J., Wirp, A., Kip, D., Krätzig, E. & Berben, D. (2002). *J. Opt. Soc. Am. B*, **19**, 1822–1829.
Kong, Y., Wu, S., Liu, S., Chen, S. & Xu, J. (2008). *Appl. Phys. Lett.* **9**, 251107.
Kushwaha, S. K., Maurya, K. K., Vijayan, N. & Bhagavannarayana, G. (2011). *CrystEngComm*, **13**, 4866–4872.
Kushwaha, S. K., Maurya, K. K., Vijayan, N., Kumar, B., Bhatt, R., Ganesamoorthy, S. & Bhagavannarayana, G. (2012). *CrystEngComm*, **14**, 3297–3305.
Lal, K. & Bhagavannarayana, G. (1989). *J. Appl. Cryst.* **22**, 209–215.
Lee, M., Gyoo Kim, I., Takekawa, S., Furukawa, Y., Uchida, Y., Kitamura, K. & Hatano, H. (2001). *J. Appl. Phys.* **89**, 5311–5317.
Marinova, V., Hsieh, M. L., Huei Lin, S. & Yuh Hsu, K. (2002). *Opt. Commun.* **203**, 377–384.
Marinova, V., Lin, S. H., Hsu, K. Y., Hsieh, M. L., Gospodinov, M. & Sainov, V. (2003). *J. Mater. Sci. Mater. Electron.* **14**, 857–858.
Mignoni, S., Fontana, M. D., Bazzan, M., Ciampolillo, M. V., Zaltron, A. M., Argiolas, N. & Sada, C. (2010). *Appl. Phys. B*, **101**, 541–546.
Pracka, I., Bajor, A. L., Kaczmarek, S. M., Swirkowicz, M., Kaczmarek, B., Kisielewski, J. & Lukasiewicz, T. (1999). *Cryst. Res. Technol.* **34**, 627–634.
Ramaz, F., Rakitina, L., Gospodinov, M. & Briat, B. (2005). *Opt. Mater.* **27**, 1547–1559.
Riscob, B., Bhatt, R., Vijayan, N., Bhaumik, I., Ganesamoorthy, S., Wahab, M. A., Rashmi & Bhagavannarayana, G. (2013). *J. Appl. Cryst.* **46**, 601–609.
Riscob, B., Bhaumik, I., Ganesamoorthy, S., Bhatt, R., Vijayan, N., Karnal, A. K., Wahab, M. A. & Bhagavannarayana, G. (2013). *J. Appl. Cryst.* **46**, 1854–1862.
Riscob, B., Shakir, M., Vijayan, N., Maurya, K. K., Wahab, M. A. & Bhagavannarayana, G. (2012). *J. Appl. Cryst.* **45**, 679–685.
Riscob, B., Shkir, M., Ganesh, V., Vijayan, N., Maurya, K. K., Kishan Rao, K. & Bhagavannarayana, G. (2014). *J. Alloys Compd.* **588**, 242–247.
Schlarb, U., Klauer, S., Wesselmann, M., Betzler, K. & Wohlecke, M. (1993). *Appl. Phys. A*, **56**, 311–315.
Senthi Kkumar, K., MoortyBabu, S. & &Bhagavannarayana, G. (2011). *J. Appl. Cryst.* **44**, 313–318.
Sidorov, N. V., Palatnikov, M. N., Gabrielyan, V. T., Chufyrev, P. G. & Kalinnikov, V. T. (2007). *Inorg. Mater.* **43**, 60–67.
Taue, J. C. (1972). *Optical Properties of Solids*, p. 362. Amsterdam: North-Holland.
Yang, C. H., Zhao, Y. Q., Wang, R. & Li, M. H. (2000). *Opt. Commun.* **175**, 247–252.
Yang, Y. P., Psaltis, D., Luennemann, M., Berben, D., Hartwig, U. & Buse, K. (2003). *J. Opt. Soc. Am. B*, **20**, 1491–1502.
Zaitseva, N. & Carman, L. (2001). *Prog. Cryst. Growth Charact. Mater.* **43**, 1–118.